TABLE OF CONTENTS (TOC)

High Entropy Spinel Oxide for Efficient Electrochemical Oxidation of Ammonia

Shi He[1], Vasishta Somayaji[1], Mengdi Wang[1], Seung-Hoon Lee[1], Zhijia Geng[1], Siyuan Zhu[1], Peter Novello[1], Chakrapani V. Varanasi[2], and Jie Liu[1*]

[1]Department of Chemistry, Duke University, Durham, NC 27708, United States

[2]U.S. Army Research Office P.O. Box 12211, Research Triangle Park, NC 27709, United States

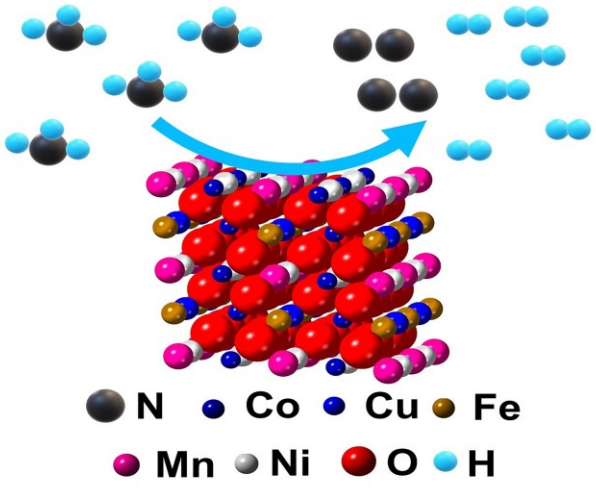

This work introduces a new family of earth-abundant transition metal high entropy oxide electrocatalysts for AOR, thus heralding a new paradigm of catalyst design for enabling ammonia as an energy carrier.

Nano Research

ISSN 1998-0124 CN 11-5974/O4
https://doi.org/(automatically inserted by the publisher)

High Entropy Spinel Oxide for Efficient Electrochemical Oxidation of Ammonia

Shi He[1], Vasishta Somayaji[1], Mengdi Wang[1], Seung-Hoon Lee[1], Zhijia Geng[1], Siyuan Zhu[1], Peter Novello[1], Chakrapani V. Varanasi[2], and Jie Liu[1,](✉)

[1]*Department of Chemistry, Duke University, Durham, NC 27708, United States*
[2]*U.S. Army Research Office P.O. Box 12211, Research Triangle Park, NC 27709, United States*

Received: day month year / **Revised:** day month year / **Accepted:** day month year (automatically inserted by the publisher)

ABSTRACT

Ammonia has emerged as a promising energy carrier owing to its carbon neutral content and low expense of long-range transportation. Therefore, development of a specific pathway to release the energy stored in ammonia is therefore in urgent demand. Electrochemical oxidation provides a convenient and reliable route to attain efficient utilization of ammonia. Here, we report that the high entropy (Mn, Fe, Co, Ni, Cu)$_3$O$_4$ oxides can achieve high electrocatalytic activity for the ammonia oxidation reaction (AOR) in non-aqueous solutions. The AOR onset overpotential of (Mn, Fe, Co, Ni, Cu)$_3$O$_4$ is 0.70 V, which is nearly 0.2 V lower than that of their most active single metal cation counterpart. The mass spectroscopy study revealed that (Mn, Fe, Co, Ni, Cu)$_3$O$_4$ preferentially oxidizes ammonia to environmentally friendly diatomic nitrogen with a Faradic efficiency of over 85%. The XPS result indicates that the balancing metal d-band of Mn and Cu cations helps retain a long-lasting electrocatalytic activity. Overall, this work introduces a new family of earth-abundant transition metal high entropy oxide electrocatalysts for AOR, thus heralding a new paradigm of catalyst design for enabling ammonia as an energy carrier.

KEYWORDS

Type keywords (4 to 6 keywords) here. The font is Helvetica 9

1. Introduction

One of the main problems facing our planetary bodies is unexpected and sudden climate change due to continuously increasing fossil fuel consumption. Developing clean and renewable energy sources provides an attractive solution to displace carbon-intensive fossil fuels and decrease carbon dioxide emissions from burning fossil fuel [1]. Among many prospective renewable and clean energy sources, ammonia has been considered a promising candidate because of its carbon neutral content, high energy density, low flammability, ease of liquefaction and the vast availability of existing infrastructure [2]. Furthermore, there is a growing progress in scalable ammonia synthesis relying on renewable sources of energy, which causes ammonia to economically compete with other energy resources [3-6]. In order to further realize an efficient strategy to utilize NH_3, electrochemical oxidation of NH_3 is a promising approach that directly converts solar energy stored in NH_3 into electricity at room temperature [7]. During the electrochemical oxidation of NH_3, the key process at the electrode and electrolyte interface involves multiple electron transfer events from the active site to the adsorbed ammonia molecule and finally preferentially forming an environmentally friendly dinitrogen product. Even though the standard electrochemical potential of converting NH_3 to N_2 is around 0.1 V vs. NHE [8], kinetic sluggish N-N bond formation and desorption of the final $*N_{2ad}$ to generate N_2 lead to a large energy barrier during the ammonia oxidation reaction(AOR) [9]. Therefore, it is imperative to develop a new family of electrocatalysts to reduce the energy barrier of N-N bond formation and accelerate desorption of the final $*N_{2ad}$.

Over the past few decades, several efforts have been made to reduce the kinetic barriers and enhance the selectivity of oxidizing ammonia dissolved in aqueous medium.[10] For example, Pt(100) facet showed an approximately 0.55 V onset overpotential for catalyzing AOR with a maximum current density of 1.1 mA/cm^2 [10]. However, this electrocatalyst has only a 0.2 V potential window to avoid the accumulation of nitrate poisonous species [10]. Additionally, electrochemically deposited NiO catalysts need about 1.3 V onset overpotential for AOR with 10% of ammonia oxidized to NO_3^- at 30mA/cm^2 in aqueous medium [11]. Therefore, the narrow potential window and the formation of nitrate byproducts in aqueous media limit the current density and selectivity of AOR [12]. To overcome these limitations in aqueous solvent, many recent studies have shifted to NH_3 electrolysis in non-aqueous solutions [13, 14]. Although the electrochemically

Address correspondence to Jie Liu, *Email: j.liu@duke.edu

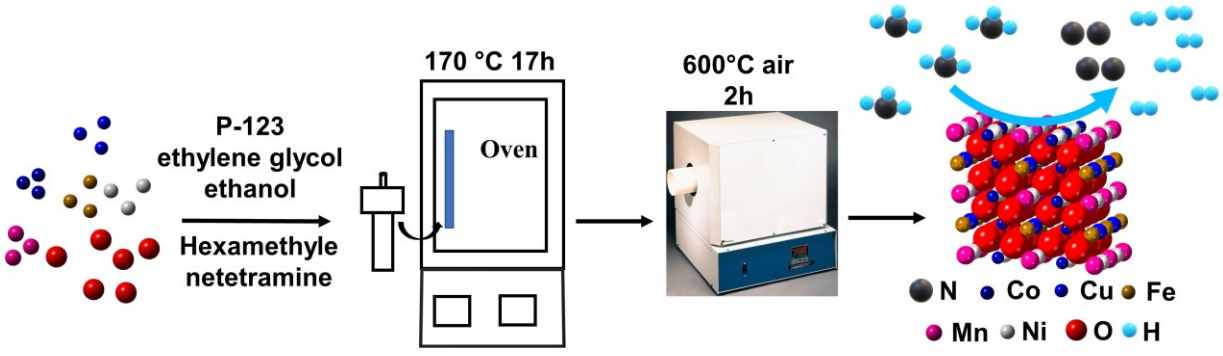

Scheme 1. Schematic representations of synthesis route of $((Mn, Fe, Co, Ni, Cu)_3O_4$ where the size of each atom represents its ionic radius.

deposited Pt nanoparticle initially showed good AOR performance in NH_3 saturated acetonitrile solutions,[15] the activity quickly decreased due to the formation of a nitridation layer on the Pt surface [16]. The stainless steel anode worked at higher voltages [17], but the electrode materials were found to corrode by the solvent to form $Fe(NH_3)_6Cl_2$. Usually, the poisoning of electrocatalysts is considered a key factor affecting the rate limiting steps in AOR [13, 18, 19]. Consequently, designing an active and stable electrocatalyst with reasonable NH_3 adsorption/desorption sites is crucial to achieving a low overpotential and high current for AOR. In general, the nature of scaling relations creates a volcano curve based on Sabatier's principle in which the optimal catalyst surface has neither too strong nor too weak adsorption and is found at the apex [20-25]. The moderate adsorption on an optimal catalyst in electrochemical reactions represents a balance between rates of the dissociative adsorption of reactants and the desorption of intermediates and products. However, as heterogeneous catalytic reactions on metal surfaces involve complex networks of elementary steps, it is impossible to manipulate and enhance a single elementary step without affecting the energetics of all the other elementary steps [26]. Many efforts have been put on solving this paradoxical problem, including alloying metals from opposite sides of the volcano curve to achieve an optimum. However, the number of available alloys is limited by the miscibility of metal ions, so few of the combination of elements can form a homogeneous alloy. Additionally, most of the alloys are prone to form separated phases during the catalysis process which shortens the catalyst lifetime. Recently, a new class of materials called high entropy materials (HEMs) was discovered, which enables straightforward control of the electronic structure by changing the element atomic ratio in the homogeneous crystal [27]. To date, high entropy alloys, metal oxides, metal nitrides, metal carbides, metal diborides, metal halides, and metal chalcogenides has been synthesized [28-31]. Instead of simply blending each metal cation, different atoms with different d-band structure in HEM will merge uniformly into a single-phase crystal that allows for attaining a unique d-band structure with abundant active sites [27, 29, 32]. More recently, HEM have been extensively utilized as catalysts in water splitting, CO_2 reduction, anode material for lithium ion battery and supercapacitor.[33, 34] These materials therefore can construct an uniform active phase with different metal atoms to achieve synergistic effect between different metal cations [35, 36]. As a result, high entropy materials is quickly becoming an active research direction in materials research and can be the prominent candidates for multistep reaction such as the activation of N-H bonds and desorption of the N-N product together.

To maximize the efficiency and stability of transition metal oxide electrocatalysts for AOR, we designed high entropy spinel $(Mn, Fe, Co, Ni, Cu)_3O_4$ electrocatalysts in this work. This equiatomic metal oxide was synthesized by using layered double hydroxide as a mediator to form an entropy driven homogenous spinel structure (Scheme 1). The electrocatalytic activity of the high entropy spinel $(Mn, Fe, Co, Ni, Cu)_3O_4$ exhibits a substantially lower onset overpotential for AOR than its single cation counterpart with a Faradic efficiency of N_2 production over 90%. The XPS study revealed that moderate nitrogen binding strength was probably achieved by controlling electronic structure of Mn and Cu active sites and is responsible for the optimized performance because it benefits key reaction steps in AOR, including the generation of the NH_x^+ cation radical, as well as the adsorption of NH_3 and desorption of the final $*N_2$ species.

2. Experimental Information

Synthesis of high entropy oxide ((Mn, Fe, Co, Ni, Cu)$_3$O$_4$): As shown in Scheme 1$(Mn, Fe, Co, Ni, Cu)_3O_4$ was prepared by a modified method from Ref. [37-39] which use layered double hydroxides (LDHs) as precursor. In a typical synthesis, 0.3 g polyethyleneoxide – polypropyleneoxide – polyethylene oxide (PEO20–PPO70–PEO20, Pluronic P123) was dissolved in 15 mL ethanol, then 10 mL H_2O, and 45 mL ethylene glycol were added to form a homogeneous solution. Next, 0.3mmol $Co(Ac)_2{\cdot}4H_2O$, 0.3mmol $Ni(Ac)_2{\cdot}4H_2O$, 0.3mmol $Mn(Ac)_2{\cdot}4H2O$, 0.3mmol $Fe(Ac)_2$, 0.3mmol $Cu(Ac)_2{\cdot}H_2O$ and 0.21 g hexamethylenetetramine (HMTA) were added into the mixed solution under vigorous stirring for 45 min. After that, the solution was transferred into a 100 mL stainless-steel Teflon-lined autoclave and heated at 170 °C for 15 h. It was then cooled to room temperature, and the product was washed several times with water and ethanol before dried at 60 °C, yielding the high entropy hydroxide precursor. The HEO nanoparticles were obtained by calcinating the precursor at 600 °C for 2h.

Electrochemical Measurement: The AOR Electrode was fabricated from a mixture of 5 mg as-prepared high entropy oxide, and 5 mg of carbon powder (Vulcan XC-72) dispersed in solvent containing 0.5 mL of water, 0.5 mL of isopropyl alcohol, and 17.5 μL of neutralized Nafion solution (5 wt %, Sigma-Aldrich). After thorough sonication, 20 μL of the catalyst ink was pipetted on the carbon fiber paper (CFP), which was air-dried to obtain a mass loading of 0.1 mg oxide/cm^2. Cyclic voltammetry (CV) was

performed in a three-electrode configuration in 0.10 M KPF_6 acetonitrile solution using catalysts coated CFP as the working electrode, Ag/Ag^+ as the reference electrode and Pt mesh as the counter electrode. The potential of Ag/Ag^+ was calibrated by the method in previous report.[16] The solution was saturated with NH_3 (UHP, Airgas) for 30 min before measuring the catalyst activities. The background currents were also collected by purging the solution with Ar for 30 min and then measuring under the same conditions.

A chronopotentiometry test was performed in the same three electrode system using NH_3 saturated 0.10 M KPF_6 acetonitrile solution with continuous flow NH_3 over the electrolyte during the test. The potential was set at 1.0 V vs NHE during the measurement.

Electrochemical impedance spectroscopy (EIS): The EIS test was conducted using a Bio-Logic SP300 electrochemical workstation. The EIS measurements were carried out in NH_3 saturated 0.10 M KPF_6 acetonitrile solution at 1.0 V vs NHE. The spectra were collected in the frequency range from 0.10 to 100 kHz with an amplitude of 10 mV.

Characterization of structure and chemical states: Powder x-ray diffraction (XRD) patterns were collected on a Panalytical X'Pert PRO MRD HR XRD diffractometer with Cu Kα radiation. The XRD pattern was refined by the HighScore Plus Rietveld refinement program. SEM images were taken with a FEI XL30 SEM-FEG microscope (operating voltage, 7 kV). The X-ray photoelectron spectroscopy (XPS) was performed by a Kratos Analytical Axis Ultra system, and all the spectra were calibrated to the C 1s transition set at 284.8 eV. The Transmission electron microscopy (TEM) images were collected by a FEI Tecnai G2 Twin operating at 200 kV. The TEM samples were prepared by dispersing the electrocatalysts in ethanol under sonication anddepositing on a copper grid coated with a carbon film (Ted Pella, 01813). The size of nanoparticles was further determined with Digital Instruments Dimension 3100 atomic force microscopy (AFM) by drop-casting of nanoparticle suspension on silicon wafer substrate.

3. Results and Discussion

As shown in Scheme 1. The (Mn, Fe, Co, Ni, Cu)$_3O_4$ was prepared by a precursor morphology-directed strategy using metal LDH as precursors, and then LDH was annealed in air at 600°C to obtain (Mn, Fe, Co, Ni, Cu)$_3O_4$. The structures of (Mn, Fe, Co, Ni, Cu)$_3O_4$ was investigated by X-ray diffraction (XRD). Before the calcination, the precursor displays unresolved diffraction peaks at the range of 33°-34° and 42°-43°, indicating mixing of many different phase. After calcination at 600C for 2h, the XRD pattern of (Mn, Fe, Co, Ni, Cu)$_3O_4$ displays seven major diffraction peaks at 30.9°, 35.7°.38.5°,43.9°, 54.3°,57.9°,63.9°, which could be well indexed to (220), (331), (222), (400), (422), (511) and (440) planes of the spinel Co_3O_4 (Fd3m) structure with standard powder diffraction card number ICDD 01-076-1802. The broadening of diffraction peak could be ascribed to the strong lattice distortion and nanometer size of (Mn, Fe, Co, Ni, Cu)$_3O_4$ particle [39, 40]. Obviously, this result indicates the Co, Cu, Fe, Mn, Ni-based product exhibited a single-phase, the Fd3m spinel structure, which is in line with (Mn, Fe, Co, Ni, Cu)$_3O_4$ stoichiometry. Detailed morphologies of (Mn, Fe, Co, Ni, Cu)$_3O_4$ were further examined by SEM, TEM, and AFM. In Figure 1b and Figure S1, SEM and TEM image demonstrates that the average size of (Mn, Fe, Co, Ni, Cu)$_3O_4$ is about 10 - 20 nm with a nanosphere like morphology. Chemical compositions of these (Mn, Fe, Co, Ni, Cu)$_3O_4$ was further investigated by using energy dispersive X-ray (EDX) and elemental mapping as shown in Figure S2. Each element of Mn, Fe, Co, Ni, Cu disperses uniform across the whole region, implying the homogeneous distribution of each element in (Mn, Fe, Co, Ni, Cu)$_3O_4$ crystal. The EDX results in Figure S2 further show that the

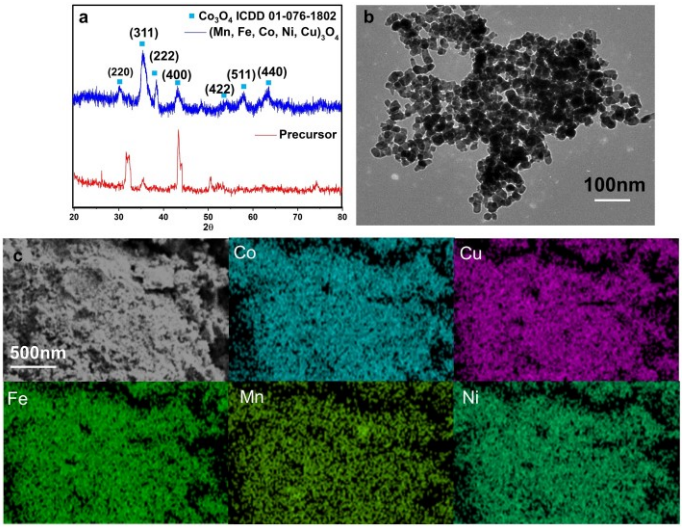

Figure 1. (a) X-ray diffraction patterns of (Mn, Fe, Co, Ni, Cu)$_3O_4$ which is well indexed to the spinel Co_3O_4 ICDD 01-076-1802 with Fd3m structure; (b)TEM image of (Mn, Fe, Co, Ni, Cu)$_3O_4$ and (c) SEM image and its corresponding element mapping of Ni, Mn, Co, Fe, and Cu.

existence of all the metal cation atoms in the (Mn, Fe, Co, Ni, Cu)$_3O_4$ crystal and they have nearly equiatomic ratio. Summarizing of all of above results, we have successfully prepared high entropy (Mn, Fe, Co, Ni, Cu)$_3O_4$. The size and morphologies of (Mn, Fe, Co, Ni, Cu)$_3O_4$ nanoparticle were further characterized by AFM. It demonstrates the size of (Mn, Fe, Co, Ni, Cu)$_3O_4$ nanoparticle ranges from 5 to15 nm, which is consistent to the size obtained by TEM and SEM images.

The electrocatalytic properties of (Mn, Fe, Co, Ni, Cu)$_3O_4$ and its single metal cation spinel materials were evaluated by cyclic voltammetry (CV) and linear scan voltammetry (LSV). As shown in Figure 2a and Figure S6a, the (Mn, Fe, Co, Ni, Cu)$_3O_4$ exhibits substantially higher activity than other tested single metal cation spinel electrocatalysts. This onset overpotential is about 0.2 V lower than that of the most active single metal cation Mn_3O_4 electrocatalyst under similar electrocatalytic conditions. The (Mn, Fe, Co, Ni, Cu)$_3O_4$ also achieves a current density of 10 mA/cm^2 at 1.15 V vs. NHE and can reach 15 mA/cm^2 at 1.2 V vs. NHE. Moreover, the AOR mass activity of (Mn, Fe, Co, Ni, Cu)$_3O_4$ in Figure 2b is 44 mA/cm^2/mg. This mass activity is approximately 2 times that of Mn_3O_4 electrocatalyst. To the best of our knowledge, this is the first report that high entropy oxide can be a highly efficient electrocatalyst with high AOR performance with respect to current density and overpotential (displayed in Figure 2a and Table S1). More interestingly, Figure 2c illustrates that (Mn, Fe, Co, Ni, Cu)$_3O_4$ retains over 90% of the initial current density after 1h reaction. The stability of (Mn, Fe, Co, Ni, Cu)$_3O_4$ were further examined by repeated chronoamperometry and cyclic voltammetry experiments. The AOR current density of (Mn, Fe, Co, Ni, Cu)$_3O_4$

Nano Research
ISSN 1998-0124 CN 11-5974/O4
https://doi.org/(automatically inserted by the publisher)

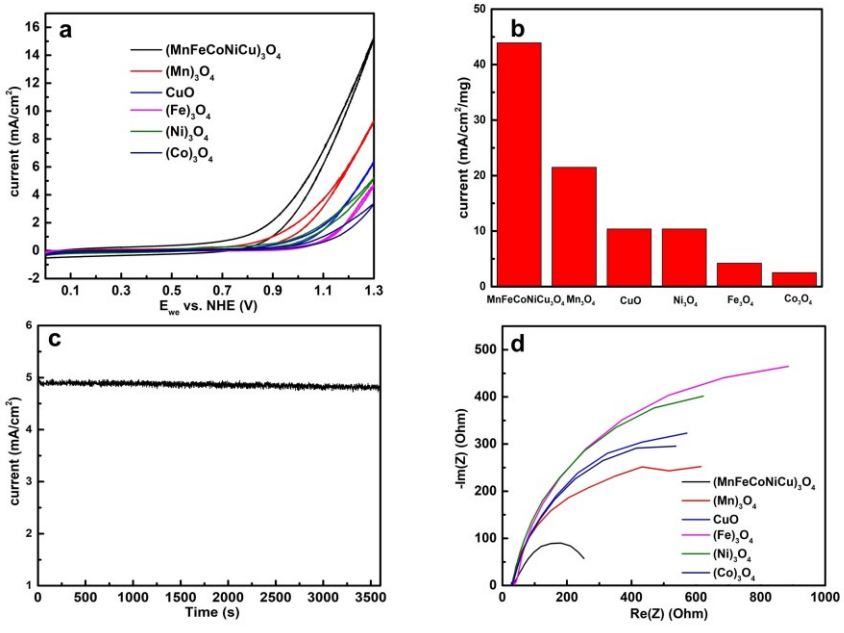

Figure 2. (a) Cyclic voltammetry of (Mn, Fe,Co, Ni, Cu)$_3O_4$ and its single metal cation counterparts in saturated 0.1M KPF_6 acetonitrile solution without any IR correction; (b) Mass activity of (Mn, Fe, Co, Ni, Cu)$_3O_4$ and its single metal cation counterpart at 1.0V vs NHE. (c) Chronoamperometric profiles of (Mn, Fe, Co, Ni, Cu)$_3O_4$ in NH_3 saturated 0.1M KPF_6 acetonitrile solution at 1.0V vs NHE; (d) Nyquist plots of (Mn, Fe, Co, Ni, Cu)$_3O_4$ and its single metal cation counterparts in NH_3 saturated 0.1M KPF_6 acetonitrile solution at 1.0V vs NHE.

in Figure S6b can maintain above 90% of its initial current density after three times continuous 1h chronoamperometry tests at 1.05, 0.95, and 0.90 V vs. NHE, indicating high catalytic stability of electrocatalysts during the AOR process. XRD analysis of (Mn, Fe, Co, Ni, Cu)$_3O_4$ was performed before and after the AOR process to examine any possible phase changes, where no obvious shift of diffraction peaks in the XRD pattern (Figure S3) was observed. This result suggests that the structure of (Mn, Fe, Co, Ni, Cu)$_3O_4$ is stable during AOR process. Compared with the every single metal cation spinel oxide in Figure 2d, the small semicircle in (Mn, Fe, Co, Ni, Cu)$_3O_4$ represents a small charge-transfer resistance R_{ct}, implying that the increase of charge transfer rate favors for enhancing the AOR activity [41].

Additionally, to examine the AOR products, we used mass spectroscopy to analyze the gaseous products during the AOR process as shown in Figure S4a. The calculated results from these data are illustrated in Figure 3a, b. They demonstrated a high nitrogen production rate of more than 7.2mmol/mg/s with FE over

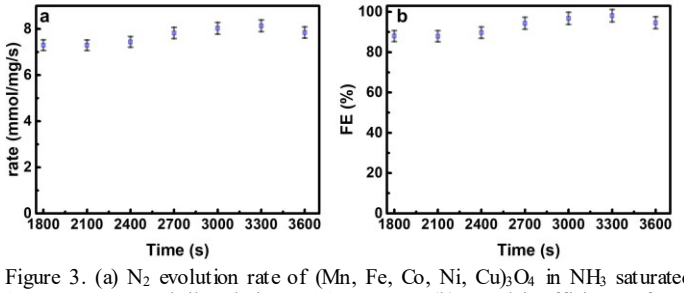

Figure 3. (a) N_2 evolution rate of (Mn, Fe, Co, Ni, Cu)$_3O_4$ in NH_3 saturated 0.1M KPF_6 acetonitrile solution at 1.0 V vs RHE (b) Faradaic efficiency of N_2.

90% at 1.0 V vs. NHE for (Mn, Fe, Co, Ni, Cu)$_3O_4$. Furthermore, we studied the formation of hydrazine by a reported colorimetric method [42], as shown in Figure S4b. The absence of absorption peak at around 456 nm indicated that there is no hydrazine formation during the AOR process using (Mn, Fe, Co, Ni, Cu)$_3O_4$ as the electrocatalyst.

We also analyzed the chemical states of all metal atoms by the XPS. As shown in Figure 4a, the XPS peaks of Co $2p_{3/2}$ in the (Mn, Fe, Co, Ni, Cu)$_3O_4$ was centered at 780.5 eV. The Co $2p_{3/2}$ peak can be deconvoluted with a main peak at 781.9 eV and a peak at 780.4 eV, which can be assigned to Co^{2+} and Co^{3+} [43-45]. In the region scan of Fe 2p XPS spectra in Figure 4b, the $2p_{3/2}$ peak was centered at 711.3 eV. The two fitted peaks for Fe $2p_{3/2}$ are attributed to Fe^{3+} (712.7 eV) and Fe^{2+} (710.9 eV), respectively [46]. For Ni 2p in Figure 4c, the $2p_{3/2}$ peak was centered at 854.9 eV. The fitted peaks at 854.7 and 856.2 eV can be assigned to Ni^{2+} and Ni^{3+} of its $2p_{3/2}$ respectively. Compared to their single cation spinel oxide, no significant difference can be found for the XPS spectra of Fe, Co, and Ni. Interestingly, the Mn $2p_{3/2}$ peak of (Mn, Fe, Co, Ni, Cu)$_3O_4$ in Figure 4d locates at 641.3 eV and a clear blueshift can be observed in the Mn $2p_{3/2}$ region compared to that of Mn_3O_4 which locates at around 639.6 eV. Further peak deconvolution analysis of Mn $2p_{3/2}$ demonstrates that the ratio of Mn^{4+} (642.1 eV) to Mn^{2+} (640.7 eV) is 1.3 while it is 0.8 in Mn_3O_4. This result indicates that more percentage of Mn atoms are occupied in octahedral sites in (Mn, Fe, Co, Ni, Cu)$_3O_4$ [47]. The Cu 2p XPS spectra of the (Mn, Fe, Co, Ni, Cu)$_3O_4$ samples are also shown in Figure 4e. The center of Cu $2p_{3/2}$ spectrum of (Mn, Fe, Co, Ni, Cu)$_3O_4$ were resolved into two peaks at 933.4 eV and 934.5 eV respectively. The signal with low binding energy (933.4 eV) was attributed to Cu^+, and the signal at high binding energy (934.5 eV) was indicative of Cu^{2+} along with its satellite from 938.0 to 948.0 eV. The ratio of Cu^+ to Cu^{2+} on the surface of (Mn, Fe, Co, Ni, Cu)$_3O_4$ is 3:1. However,

negligible Cu^+ can be found in CuO.

In this study, the most important result was activity, selectivity and stability of the $(Mn, Fe, Co, Ni, Cu)_3O_4$ during the AOR are substantially improved compared to that of their counterpart single metal material. The interaction between each metal cations has benefits for enhancing the AOR catalytic performance. At first, according to the d-band theory,[48] the valence electron filling of

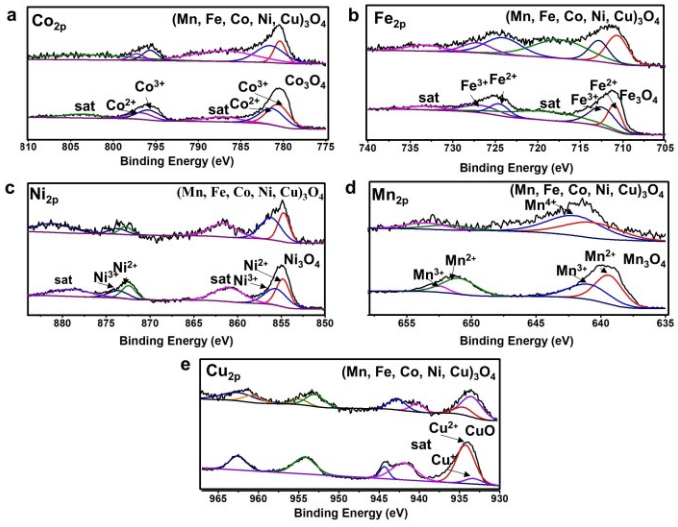

Figure 4. XPS spectra of $(Mn, Fe, Co, Ni, Cu)_3O_4$ and its single metal cation counterparts (a) Co_{2p}, (b) Fe_{2p}, (c) Ni_{2p}, (d) Mn_{2p}, (e) Cu_{2p}.

metal-adsorbate antibonding states is governed by the metal d-band center relative to its Fermi level. Our XPS study in Figure 4 demonstrates that the concentration of Mn^{3+} and Cu^+ in $(Mn, Fe, Co, Ni, Cu)_3O_4$ are higher than their single metal cation counterpart. The increase of Mn^{3+} will downshift d-band center of Mn which will have a weaker metal-adsorbate bond compared to the Mn_3O_4 while the increase of Cu^+ will upshift of the d-band center of Cu will result in the stronger binding of ammonia. However, previous calculation studies have showed that the adsorption of ammonia on Mn site was too strong in manganese oxide and a weak adsorption of ammonia was found on the surface of Cu in CuO [49, 50]. We consider that the d-band center of Mn and Cu in $(Mn, Fe, Co, Ni, Cu)_3O_4$ therefore would attain a moderate metal ammonia bond strength, so that it optimizes the key steps in AOR including adsorption of NH_3 and desorption of final $*N_2$ species, in accordance with correlation between N species binding energy and metal d-band electronic structure in previous reports [13, 48, 51]. Also, the high entropy effect can help the dispersion of each metal cations which forms a homogeneous solid solution and expose a greater number of sites. A similar effect that combination of this ensemble and charge transfer between metal cations have also been observed in high-entropy fluorite oxide [52].

4. Conclusion

In summary, we studied the use of high entropy spinel $(Mn, Fe, Co, Ni, Cu)_3O_4$ oxide as AOR electrocatalysts toward efficient N_2 generation. $(Mn, Fe, Co, Ni, Cu)_3O_4$ shows 0.7 V onset overpotential which is 0.15 V lower than that of the most active single metal oxide, more than 90% N_2 selectivity, and a high 15 mA/cm^2 current density at 1300 mV vs. NHE. The current density of $(Mn, Fe, Co, Ni, Cu)_3O_4$ also retains above 90% after 1 h constant AOR. The XPS study clearly shows the difference of electronic structure of Cu and Mn atom in $(Mn, Fe, Co, Ni, Cu)_3O_4$ compared to that of their single metal counterparts, which can probably promote the formation of NH_x^+ cation radical and suppresses the side reaction of generating soluble metal-ammonia complex for achieving a high yield of oxidizing ammonia to N_2. This research opens up an opportunity to directly engineer atomic composition of nanomaterial for a high-performance electrochemical oxidation of ammonia.

Competing Interest

The authors have declared that no competing interest exists.

Acknowledgements

This research is partially supported by the Energy Research Seed Grant from Duke Energy Initiative, the National Science Foundation (CHE-1565657. CHE-1954838) and the Army Research Office (W911NFN-18-2-004). S.H. and P.N. are both supported by fellowships from Department of Chemistry at Duke University. This work was performed in part at the Duke University Shared Materials Instrumentation Facility (SMIF), a member of the North Carolina Research Triangle Nanotechnology Network (RTNN), which is supported by the National Science Foundation (award number ECCS-2025064) as part of the National Nanotechnology Coordinated Infrastructure (NNCI).

Electronic Supplementary Material: Supplementary material (Additional TEM image, EDS spectra, and XRD after reaction of $(Mn, Fe, Co, Ni, Cu)_3O_4$, Mass spectra for AOR product determination, UV-Vis spectra for the hydrazine determination) is available in the online version of this article.

References

[1] Møller, K. T.; Jensen, T. R.; Akiba, E.; Li, H.-w. Hydrogen - a sustainable energy carrier. *Progress in Natural Science: Materials International* **2017,** *27*, 34-40.

[2] Xue, M.; Wang, Q.; Lin, B.-L.; Tsunemi, K. Assessment of ammonia as an energy carrier from the perspective of carbon and nitrogen footprints. *ACS Sustainable Chem. Eng.* **2019,** *7*, 12494-12500.

[3] Xue, X.; Chen, R.; Yan, C.; Zhao, P.; Hu, Y.; Zhang, W.; Yang, S.; Jin, Z. Review on photocatalytic and electrocatalytic artificial nitrogen fixation for ammonia synthesis at mild conditions: Advances, challenges and perspectives. *Nano Research* **2019,** *12*, 1229-1249.

[4] Ma, B.; Zhao, H.; Li, T.; Liu, Q.; Luo, Y.; Li, C.; Lu, S.; Asiri, A. M.; Ma, D.; Sun, X. Iron-group electrocatalysts for ambient nitrogen reduction reaction in aqueous media. *Nano Research* **2021,** *14*, 555-569.

[5] Liu, Y.; Huang, L.; Fang, Y.; Zhu, X.; Dong, S. Achieving ultrahigh electrocatalytic nh3 yield rate on fe-doped bi2wo6 electrocatalyst. *Nano Research* **2021**.

[6] Li, S.; Wang, Y.; Liang, J.; Xu, T.; Ma, D.; Liu, Q.; Li, T.; Xu, S.; Chen, G.; Asiri, A. M. et al. Tib2 thin film enabled efficient nh3 electrosynthesis at ambient conditions. *Materials Today Physics* **2021,** *18*, 100396.

[7] Umeyama, T.; Tezuka, N.; Kawashima, F.; Seki, S.; Matano, Y.; Nakao, Y.; Shishido, T.; Nishi, M.; Hirao, K.; Lehtivuori, H. et al. Carbon nanotube wiring of donor–acceptor nanograins by self-assembly and efficient charge transport. *Angew. Chem. Int. Ed.* **2011,** *50*, 4615-4619.

[8] Adli, N. M.; Zhang, H.; Mukherjee, S.; Wu, G. Review—ammonia oxidation electrocatalysis for hydrogen generation and fuel cells. *J. Electrochem. Soc.* **2018,** *165*, J3130-J3147.

[9] Siddharth, K.; Chan, Y.; Wang, L.; Shao, M. Ammonia electro-oxidation reaction: Recent development in mechanistic understanding and electrocatalyst design. *Curr. Opin. Electrochem* **2018,** *9*, 151-157.

[10] Katsounaros, I.; Figueiredo, M. C.; Calle-Vallejo, F.; Li, H.; Gewirth, A. A.; Markovic, N. M.; Koper, M. T. M. On the mechanism of the electrochemical conversion of ammonia to dinitrogen on pt(1 0 0) in alkaline environment. *J. Catal.* **2018,** *359*, 82-91.

[11] Almomani, F.; Bhosale, R.; Khraisheh, M.; Kumar, A.; Tawalbeh, M. Electrochemical oxidation of ammonia on nickel oxide nanoparticles. *Int. J. Hydrogen Energy* **2020,** *45*, 10398-10408.

[12] Shih, Y.-J.; Huang, Y.-H.; Huang, C. P. In-situ electrochemical formation of nickel oxyhydroxide (niooh) on metallic nickel foam electrode for the direct oxidation of ammonia in aqueous solution. *Electrochim. Acta* **2018,** *281*, 410-419.

[13] Schiffer, Z. J.; Lazouski, N.; Corbin, N.; Manthiram, K. Nature of the first electron transfer in electrochemical ammonia activation in a nonaqueous medium. *J. Phys. Chem. C* **2019,** *123*, 9713-9720.

[14] He, S.; Chen, Y.; Wang, M.; Liu, K.; Novello, P.; Li, X.; Zhu, S.; Liu, J. Metal nitride nanosheets enable highly efficient electrochemical oxidation of ammonia. *Nano Energy* **2021,** *80*, 105528.

[15] Peng, W.; Xiao, L.; Huang, B.; Zhuang, L.; Lu, J. Inhibition effect of surface oxygenated species on ammonia oxidation reaction. *J. Phys. Chem. C* **2011,** *115*, 23050-23056.

[16] Little, D. J.; Smith, I. I. I. M. R.; Hamann, T. W. Electrolysis of liquid ammonia for hydrogen generation. *Energy Environ. Sci.* **2015,** *8*, 2775-2781.

[17] Goshome, K.; Yamada, T.; Miyaoka, H.; Ichikawa, T.; Kojima, Y. High compressed hydrogen production via direct electrolysis of liquid ammonia. *Int. J. Hydrogen Energy* **2016,** *41*, 14529-14534.

[18] Ghosh, S.; Banerjee, P.; Nandi, P. K. Heterolytic nh bond activation of ammonia by dinuclear [{m(μ-ome)}2] complexes (m = sc – v and mn – ni): A theoretical investigation. *Comput. Theor. Chem.* **2018,** *1145*, 44-53.

[19] Robinson, T. P.; De Rosa, D. M.; Aldridge, S.; Goicoechea, J. M. E–h bond activation of ammonia and water by a geometrically constrained phosphorus(iii) compound. *Angew. Chem. Int. Ed.* **2015,** *54*, 13758-13763.

[20] Medford, A. J.; Vojvodic, A.; Hummelshøj, J. S.; Voss, J.; Abild-Pedersen, F.; Studt, F.; Bligaard, T.; Nilsson, A.; Nørskov, J. K. From the sabatier principle to a predictive theory of transition-metal heterogeneous catalysis. *J. Catal.* **2015,** *328*, 36-42.

[21] Bligaard, T.; Nørskov, J. K.; Dahl, S.; Matthiesen, J.; Christensen, C. H.; Sehested, J. The brønsted–evans–polanyi relation and the volcano curve in heterogeneous catalysis. *J. Catal.* **2004,** *224*, 206-217.

[22] Greeley, J. Theoretical heterogeneous catalysis: Scaling relationships and computational catalyst design. *Annu Rev Chem Biomol Eng* **2016,** *7*, 605-35.

[23] Logadottir, A.; Rod, T. H.; Nørskov, J. K.; Hammer, B.; Dahl, S.; Jacobsen, C. J. H. The brønsted–evans–polanyi relation and the volcano plot for ammonia synthesis over transition metal catalysts. *J. Catal.* **2001,** *197*, 229-231.

[24] Wang, Z.; Wang, H.-F.; Hu, P. Possibility of designing catalysts beyond the traditional volcano curve: A theoretical framework for multi-phase surfaces. *Chem. Sci.* **2015,** *6*, 5703-5711.

[25] Norskov, J. S., F.; Abild-Pedersen, F.;Bligaard, T. *Fundamental concepts in heterogeneous catalysis*. 2010.

[26] Kale, M. J.; Avanesian, T.; Christopher, P. Direct photocatalysis by plasmonic nanostructures. *ACS Catal.* **2014,** *4*, 116-128.

[27] Miracle, D. B.; Senkov, O. N. A critical review of high entropy alloys and related concepts. *Acta Mater.* **2017,** *122*, 448-511.

[28] Zhang, Y. High-entropy materials-a brief introduction. *Springer* **2019**.

[29] George, E. P.; Raabe, D.; Ritchie, R. O. High-entropy alloys. *Nature Reviews Materials* **2019,** *4*, 515-534.

[30] Oses, C.; Toher, C.; Curtarolo, S. High-entropy ceramics. *Nature Reviews Materials* **2020,** *5*, 295-309.

[31] Zhang, R.-Z.; Reece, M. J. Review of high entropy ceramics: Design, synthesis, structure and properties. *Journal of Materials Chemistry A* **2019,** *7*, 22148-22162.

[32] Zhang, Y.; Zuo, T. T.; Tang, Z.; Gao, M. C.; Dahmen, K. A.; Liaw, P. K.; Lu, Z. P. Microstructures and properties of high-entropy alloys. *Prog. Mater Sci.* **2014,** *61*, 1-93.

[33] Sarkar, A.; Wang, Q.; Schiele, A.; Chellali, M. R.; Bhattacharya, S. S.; Wang, D.; Brezesinski, T.; Hahn, H.; Velasco, L.; Breitung, B. High-entropy oxides: Fundamental aspects and electrochemical properties. **2019,** *31*, 1806236.

[34] Löffler, T.; Savan, A.; Garzón-Manjón, A.; Meischein, M.; Scheu, C.; Ludwig, A.; Schuhmann, W. Toward a paradigm shift in electrocatalysis using complex solid solution nanoparticles. *ACS Energy Letters* **2019,** *4*, 1206-1214.

[35] Meng, H.; Wu, X.; Ci, C.; Zhang, Q.; Li, Z. J. P. i. R. K.; Mechanism A density functional theory study of nh3 and no adsorption on the#²-mno2 (110) surface. **2018,** *43*, 219 - 228.

[36] Herron, J. A.; Ferrin, P.; Mavrikakis, M. Electrocatalytic oxidation of ammonia on transition-metal surfaces: A first-principles study. *J. Phys. Chem. C* **2015,** *119*, 14692-14701.

[37] Chen, Q.; Wang, R.; Yu, M.; Zeng, Y.; Lu, F.; Kuang, X.; Lu, X. Bifunctional iron–nickel nitride nanoparticles as flexible and robust electrode for overall water splitting. *Electrochim. Acta* **2017,** *247*, 666-673.

[38] Li, M.; Jijie, R.; Barras, A.; Roussel, P.; Szunerits, S.; Boukherroub, R. Nife layered double hydroxide electrodeposited on ni foam coated with reduced graphene oxide for high-performance supercapacitors. *Electrochim. Acta* **2019,** *302*, 1-9.

[39] Wang, D.; Liu, Z.; Du, S.; Zhang, Y.; Li, H.; Xiao, Z.; Chen, W.; Chen, R.; Wang, Y.; Zou, Y. et al. Low-temperature synthesis of small-sized high-entropy oxides for water oxidation. *Journal of Materials Chemistry A* **2019,** *7*, 24211-24216.

[40] Madhavi, J. Comparison of average crystallite size by x-ray peak broadening and williamson–hall and size–strain plots for vo2+ doped zns/cds composite nanopowder. *SN Applied Sciences* **2019,** *1*, 1509.

[41] Xu, W.; Du, D.; Lan, R.; Humphreys, J.; Miller, D. N.; Walker, M.; Wu, Z.; Irvine, J. T. S.; Tao, S. Electrodeposited nicu bimetal on carbon paper as stable non-noble anode for efficient electrooxidation of ammonia. *Appl. Catal. B Environ.* **2018,** *237*, 1101-1109.

[42] Song, P.; Wang, H.; Kang, L.; Ran, B.; Song, H.; Wang, R. Electrochemical nitrogen reduction to ammonia at ambient conditions on nitrogen and phosphorus co-doped porous carbon. *Chem. Commun.* **2019,** *55*, 687-690.

[43] Zou, R.; Xu, M.; He, S.-A.; Han, X.; Lin, R.; Cui, Z.; He, G.; Brett, D. J. L.; Guo, Z. X.; Hu, J. et al. Cobalt nickel nitride coated by a thin carbon layer anchoring on nitrogen-doped carbon nanotube anodes for high-performance lithium-ion batteries. *Journal of Materials Chemistry A* **2018,** *6*, 19853-19862.

[44] Naghash, A. R.; Etsell, T. H.; Xu, S. Xrd and xps study of cu–ni interactions on reduced copper–nickel–aluminum oxide solid solution catalysts. *Chem. Mater.* **2006,** *18*, 2480-2488.

[45] Li, X.; Guan, C.; Hu, Y.; Wang, J. Nanoflakes of ni–co ldh and bi2o3 assembled in 3d carbon fiber network for high-performance aqueous rechargeable ni/bi battery. *ACS Appl. Mater. Interfaces* **2017,** *9*, 26008-26015.

[46] Jin, Z.; Lyu, J.; Zhao, Y.-L.; Li, H.; Chen, Z.; Lin, X.; Xie, G.; Liu, X.; Kai, J.-J.; Qiu, H.-J. Top–down synthesis of noble metal particles on high-entropy oxide supports for electrocatalysis. *Chem. Mater.* **2021,** *33*, 1771-1780.

[47] Vázquez-Olmos, A.; Redón, R.; Rodríguez-Gattorno, G.; Esther Mata-Zamora, M.; Morales-Leal, F.; Fernández-Osorio, A. L.; Saniger, J. M. One-step synthesis of mn3o4 nanoparticles: Structural and magnetic study. *J. Colloid Interface Sci.* **2005,** *291*, 175-180.

[48] Nørskov, J. K.; Abild-Pedersen, F.; Studt, F.; Bligaard, T. Density functional theory in surface chemistry and catalysis. *Proc. Natl. Acad. Sci.* **2011,** *108*, 937-943.

[49] Meng, H.; Wu, X.; Ci, C.; Zhang, Q.; Li, Z. A density functional theory study of nh3 and no adsorption on the β-mno2 (110) surface. **2018,** *43*, 219-228.

[50] Yin, X.; Han, H.; Kubo, M.; Miyamoto, A. Adsorption of nh3, no2 and no on copper-aluminate catalyst: An ab initio density functional study. *Theor. Chem. Acc.* **2003,** *109*, 190-194.

[51] Neta, P.; Huie, R. E.; Ross, A. B. J. J. o. P.; Data, C. R. Rate constants for reactions of inorganic radicals in aqueous solution. *J. Phys. Chem. Ref. Data* **1988,** *17*, 1027-1284.

[52] Xu, H.; Zhang, Z.; Liu, J.; Do-Thanh, C.-L.; Chen, H.; Xu, S.; Lin, Q.; Jiao, Y.; Wang, J.; Wang, Y. et al. Entropy-stabilized single-atom pd catalysts via high-entropy fluorite oxide supports. *Nat. Commun.* **2020,** *11*, 3908.